Infrared Spectroscopy and Tunneling Dynamics of the Vinyl Radical in ^{4}He Nanodroplets

Paul L. Raston, Tao Liang and Gary E. Douberly[a)]

Department of Chemistry, University of Georgia, Athens, Georgia 30602, USA

[a)] Email: douberly@uga.edu, Tele: 01-706-542-3857

Abstract

The vinyl radical has been trapped in ^{4}He nanodroplets and probed with infrared laser spectroscopy in the CH stretch region between 2850 and 3200 cm^{-1}. The assigned band origins for the CH_2 symmetric (ν_3), CH_2 antisymmetric (ν_2), and lone α-CH stretch (ν_1) vibrations are in good agreement with previously reported full-dimensional vibrational configuration interaction computations [A. R. Sharma, B. J. Braams, S. Carter, B. C. Shepler, and J. M. Bowman, J. Chem. Phys. **130**, 174301 (2009)]. For all three bands, *a*-type and *b*-type transitions are observed from the lowest symmetry allowed roconvibrational state of each nuclear spin isomer, which allows for a determination of the tunneling splittings in both the ground and excited vibrational levels. Comparisons to gas phase millimeter-wave rotation-tunneling [K. Tanaka, M. Toshimitsu, K. Harada, and T. Tanaka, J. Chem. Phys. **120**, 3604 (2004)] and high-resolution jet-cooled infrared spectra [F. Dong, M. Roberts, and D. J. Nesbitt, J. Chem. Phys. **128**, 044305 (2008)] reveal that the He solvent effect is to reduce the ground and ν_3 excited state tunneling splittings by ≈20%. This solvent-induced modification of the tunneling dynamics can be reasonably accounted for by assuming either an ≈2.5% increase in the effective barrier height along the tunneling coordinate or an ≈5% increase in the effective reduced mass of the tunneling particles.

I. Introduction

The vinyl radical ($H_2C_\beta=C_\alpha H$) is a prototype species for probing the large amplitude intramolecular dynamics of reactive intermediates that exist along reaction paths relevant to combustion chemistry. Experimental measurements[1-5] combined with theoretical predictions[6, 7] have characterized the dynamics associated with the α-CH rocking motion that carries the vinyl radical from one C_s symmetry minimum to another *via* a C_{2v} transition state. The effective barrier along this pathway is approximately 1602(20) cm^{-1},[7] leading to tunneling splittings observed in high-resolution gas phase spectra on the order of ≈0.5 cm^{-1}.[2, 3] Full-dimensional *ab initio* potential surfaces of C_2H_3 have revealed other large amplitude pathways consisting of 1,2 hydride shifts that interchange the radical center between the C_α and C_β atoms.[8] Although the barriers associated with these pathways are ten times larger (≈18000 cm^{-1}) and above the dissociation limit, recent theoretical work has nevertheless demonstrated that tunneling promoted 1,2-H atom shifts may occur at sub-μs rates at temperatures as low as 1300 K.[9] This quantum tunneling isomerization mechanism could therefore be of considerable importance under low-pressure combustion conditions, in which the collisional time scales can be as long as 1 μs. We report here the infrared (IR) spectrum of the vinyl radical in the CH stretch region, which provides reliable band origins for vibrations that have yet to be probed with high-resolution gas phase spectroscopy. Furthermore, we consider here the effect of a solvent, namely liquid He at 0.4 K, on the large amplitude dynamics of the vinyl radical.

A rich spectroscopic history exists for the vinyl radical, and a detailed account of this can be found in Ref. 7. The first high-resolution gas phase IR study of the vinyl radical was reported by Kanamori *et al*.[1] who measured the *c*-type CH_2 wagging mode near 895 cm^{-1}. This spectrum revealed two resolved component bands separated by the difference in the v=0 and v=1 tunneling splittings (0.0541(11) cm^{-1}) associated with the large amplitude α-CH rocking motion. Millimeter wave spectroscopy of pure rotational and rotational-tunneling transitions by Tanaka *et al*. provided directly the ground state tunneling splitting, namely 0.5428(1) cm^{-1}.[2] Dong *et al*.[3] reported a high-

resolution jet-cooled spectrum of the CH_2 symmetric stretch band. The jet-cooled spectrum of this ν_3 band consists of progressions of *a*-type transitions, which provide the v=0 and v=1 tunneling splitting difference for this mode, revealing a change upon vibrational excitation of 0.0716(5) cm^{-1}. *Ab initio* computations by Nesbitt *et al*.[7] support an assignment of these measured differences to an *increase* in tunneling splitting upon either CH_2 wag or symmetric stretch excitation. Indeed, the computed vibrationally adiabatic 1D potentials along the in-plane tunneling coordinate predict a strong vibrational dependence for the splitting.

There have been several assignments of C_2H_3 vibrational band origins obtained through either time-resolved FTIR emission spectra[10-12] of the nascent vibrations formed *via* the photolysis of halogenated precursors or through the FTIR absorption spectra of the radical trapped in low-temperature solid rare gas matrixes.[13-15] The assignments from the solid-Ne spectrum of Wu *et al*.[14] agree rather closely to the full-dimensional vibrational configuration interaction (VCI) computations of Bowman and co-workers, which include explicitly a five-mode vibrational coupling representation and predict the CH_2 wag and symmetric stretch band origins to within 2 cm^{-1} of the values obtained from the high-resolution spectra.[8] Nevertheless, in the solid-Ne spectra, the highest frequency CH stretch vibrations are difficult to assign due to overlapping transitions from C_2H_2 or C_2H_4, and the ν_1 (lone α-CH stretch) and ν_2 (CH_2 antisymmetric stretch) assignments differ from the VCI predictions by 33 and 62 cm^{-1}, respectively.

In the present report, we address both the question of the CH stretch band origins and the extent to which a weakly perturbing solvent affects the tunneling dynamics. The low temperature of He nanodroplets (≈0.4 K),[16] combined with a quasi-mass-selective detection scheme, provides a technique capable of disentangling the vinyl radical spectrum in the high-frequency CH stretch region from the bands due to side products (mostly acetylene or ethylene) that arise from precursor dissociation. Moreover, due to the quantum nature of liquid He at 0.4 K, the vibrational bands of small solvated molecules are often rotationally resolved. This is indeed the case for the He-solvated vinyl radical, and this allows us to obtain the associated tunneling splittings and compare these to the gas phase spectra, where available. In previous reports of He-solvated molecular systems that exhibit large-amplitude dynamics, the solvent effect

was in every case to reduce the tunneling splittings. Strong solvent-effects are observed in the spectra of $(HF)_2$ and $(HCl)_2$, where the interchange-tunneling splittings are reduced by 40% and 28%, respectively.[17-19] An 8% reduction was observed for the splitting associated with the NH_3 inversion mode,[20] and an upper limit to reduction of 6% was obtained for H_2O_2, which undergoes wide-amplitude torsional motion.[21] Some progress has been made towards understanding these solvent effects.[22-24] For example, Sarsa *et al.*[22] and Jiang *et al*.[23] carried out fixed-node diffusion Monte Carlo studies of $(HF)_2$ in small He clusters and found that as few as four He atoms residing in a belt around the C_{2h} transition state is sufficient to account for 74% of the full nanodroplet-induced reduction in the tunneling splitting. These early results suggest that the majority of the solvent-effect is due to the He density in the direct vicinity of the tunneling particles. The spectra reported here for the vinyl radical are consistent with a solvent-effect that reduces by ≈20% the tunneling splitting associated with the wide-amplitude α-CH rocking motion.

II. Experimental Methods

The details associated with the He nanodroplet isolation technique have been reviewed,[25-27] and we discuss here only those aspects relevant to the production of the vinyl radical and its spectroscopic detection. Helium nanodroplets are formed in a continuous, cryogenic nozzle expansion of He (99.9995%) through a 5 μm diameter pinhole nozzle. With the nozzle temperatures (15-17 K) and He stagnation pressures (20 to 30 bar) used here, nanodroplets are generated that contain a few thousand helium atoms on average.[28] The droplet expansion is skimmed before entering a pick-up chamber that contains an effusive pyrolysis source for the production of the vinyl radical from the pyrolytic decomposition of di-vinyl sulfone (DVS). Radicals generated in this source are picked-up by the He droplets and cooled to approximately 0.4 K.[16]

The effusive pyrolysis source consists of a heated quartz tube separated from the DVS reservoir by a fine-metering valve. The droplet beam passes ≈1 cm from the opening of the quartz tube. The pressure in the effusive source is kept near 10^{-4} Torr to

optimize for the pick-up of single molecules and to minimize radical-radical recombination reactions within the source.[29] Upon heating the tip of the quartz tube to ≈1200 K, the decomposition of DVS into two vinyl radicals and one SO_2 molecule is observed as a sudden change in the mass spectrum of the droplet beam. Figure 1 shows the evolution of the mass spectrum as the source is heated. The bottom of the figure shows the characteristic mass spectrum of the neat droplet beam, and the middle spectrum is obtained once the DVS precursor is allowed to flow through the quartz tube. Electron bombardment ionization of a droplet leads to the initial production of a He^+ ion that subsequently ionizes the embedded DVS molecule *via* the charge transfer reaction, $He^+ + DVS \rightarrow He + (DVS^+)^* \rightarrow He + DVS^+$ fragments. The major fragmentation product of this reaction is $C_2H_3^+$ (m/z=27 u). Heating the pyrolysis source to ≈1200 K leads to a sharp drop and rise in mass channels m/z=27 and m/z=26 u, respectively. Apparently the $He^+ + C_2H_3$ reaction leads mainly to the production of $C_2H_2^+$ (m/z=26 u). Assuming complete conversion of the DVS precursor to C_2H_3 and SO_2, the maximum single vinyl radical doping efficiency is estimated to be ≈24%. The remaining 76% of droplets are either devoid of dopants or have sequentially picked-up multiple molecules that either react within the droplet or interact to form a molecular cluster.

The idler wave from a continuous-wave optical parametric oscillator (OPO) is aligned to counter-propagate the He droplet beam. The tuning and calibration of this OPO system is described elsewhere.[30] Vibrational excitation of the He-solvated vinyl radical in the CH stretch region is followed by energy transfer to the droplet and the evaporation of 500-600 He atoms, leading to a reduction in the geometric/ionization cross-section of the droplet and a concomitant decrease of ion signal in mass channels derived from droplets containing a single vinyl radical. The OPO idler beam is amplitude modulated at 80 Hz, and the laser-induced modulation of ion signal in mass channel m/z=26 u is processed with a lock-in amplifier as the OPO is tuned continuously with ≈10 MHz resolution.

III. Results

Figure 2 shows a schematic energy level diagram for the vinyl radical. Here, the symmetry labeling is based on the $C_{2v}(M)$ molecular symmetry group and assumes a feasible interchange of the two H atom nuclei in the methylenic CH_2 group. This feasible interchange occurs *via* the tunneling of the lone α-CH bond from one C_s equilibrium geometry to the other through a C_{2v} transition state. In the ground vibronic manifold, rovibronic symmetries are B_2, B_1, A_1 or A_2 for K_aK_c = ee, eo, oe, or oo. Along the contortional (i.e. tunneling) coordinate, the wavefunctions are either symmetric (A_1, +) or antisymmetric (B_2, -) with respect to the interchange of the two H atom nuclei. Combining the roconvibronic and nuclear spin symmetries ($\Gamma_{ns}=3A_1\oplus B_2$), it is easily shown that the Pauli principle demands a 3:1 or 1:3 nuclear spin weight ratio for even:odd K_a levels associated with the upper (+) or lower (-) tunneling states, respectively. Upon He solvation, the high-temperature populations of the two nuclear spin isomers are cooled completely to either the 0_{00}^+ level [ortho ($\Gamma_{ns}=A_1$)] or the 0_{00}^- level [para ($\Gamma_{ns}=B_2$)]. The allowed transitions are shown as vertical arrows in Fig. 2 and are labeled as either *a*-type or *b*-type. Because the vibrationally averaged vinyl radical structure is C_s symmetry, the vibrational bands are either pure *c*-type or *a*-/*b*-hybrid bands. The lone α-CH stretch (ν_1) and the antisymmetric and symmetric CH_2 stretch (ν_2, ν_3) bands probed here are all *a*-/*b*-hybrids, each having transition dipole moment projections onto both the *a*- and *b*- inertial axes.

Previous spectroscopic studies of the vinyl radical formed *via* the UV photolysis of vinyl-halides are all consistent with the nuclear spin weights predicted by $C_{2v}(M)$ permutation inversion group theory, as discussed above.[1, 2] For the He-solvated species at 0.4 K, we expect all CH stretch bands to consist of four transitions, and within each set (either *a*-type or *b*-type), the transition from the lower tunneling level is expected to be three times as intense as the transition from the upper tunneling level, assuming the nuclear spin weights predicted above, no nuclear spin conversion on the timescale of the measurement, and equivalent oscillator strengths out of both tunneling levels. However, it is important to note that when vinyl is produced in a slit-jet discharge

expansion, the relative intensities of lines in the ν_3^+ and ν_3^- bands are not consistent with the above set of assumptions.[3] Dong *et al*. showed from high resolution spectroscopic data that a Boltzmann analysis of the line intensities indicate a 4:4 nuclear spin weight ratio for K_a=even:odd levels for both the upper and lower tunneling manifolds, presumably due to a facile interchange of all *three* H atoms within the discharge.[3] A recently reported theoretical study of 1,2 hydride shifts in vinyl radical predicts that at temperatures greater than about 1300 K, tunneling promoted 1,2-H atom migrations occur at rates on the sub-μs timescale.[9] Given that our pyrolysis source temperature is near this regime, subsequent to pyrolysis and prior to He-solvation, this mechanism may promote the feasible exchange of all three H atoms necessary to achieve this 4:4 nuclear spin weight ratio. As this ratio would be frozen out upon droplet pick-up, this exchange mechanism would lead to equal populations in the 0_{00}^+ and 0_{00}^- levels at 0.4 K. Furthermore, an anomalous ≈3:1 intensity ratio was observed in the jet-cooled spectrum for the ν_3^+ and ν_3^- bands, indicating a tunneling manifold dependent oscillator strength for the CH_2 symmetric stretch.[3] Because this effect should be unchanged in He droplets, at least for the ν_3 band, we expect the two transitions within each *a*-/*b*-type set to appear with either a 3:1 or 9:1 intensity ratio, given either a 4:4 or 3:1 ortho:para nuclear spin state ratio, respectively.

Motivated by the substantial increase in ion signal observed in mass channel m/z=26 u upon heating the pyrolysis source, our initial search for vinyl radical transitions consisted of a measurement of the depletion signal in this mass channel as the OPO was scanned from 2850-3200 cm^{-1}. This survey scan is shown in Fig. 3, and the features assigned to the vinyl radical CH stretch bands are labeled by arrows. Apparently, the pyrolysis of DVS leads to side reactions that produce ethylene, as the remaining transitions in the survey scan are almost entirely due to He-solvated C_2H_4.[31] The most intense line that we assign to vinyl is centered at 2904.020(1) cm^{-1}, which is close to the ν_3^+, $1_{01}^+ \leftarrow 0_{00}^+$ transition (2903.8841) reported by Dong *et al.* for the jet-cooled vinyl radical.[3] Figure 4 shows a difference mass spectrum obtained with the OPO fixed to the peak of this transition. The intense peak at 26 u and the absence of

other peaks indicate that this mass channel carries essentially all of the depletion signal associated with the vibrational excitation of droplets containing single vinyl radicals.

The He-solvated C_2H_3 band origins are compared in Table 1 to those reported previously. The ν_3 band origin is observed to be nominally blue-shifted (<1 cm^{-1}) from the gas phase origin,[3] and the ν_2 and ν_1 origins are in relatively good agreement with those predicted by VCI theory.[8] Moreover, the relative intensities are consistent with density functional theory (DFT) harmonic frequency computations.[3] Further support for these assignments comes from a detailed analysis of the resolved rotational fine structure for each band. The CH_2 symmetric stretching band (ν_3) is shown in Fig. 5. As expected, the band consists of four resolved transitions (Table 2), which are assigned to the predicted transitions shown on the left-hand side of the energy level diagram in Fig. 2. The *b*-type lines are approximately three times as broad as the *a*-type transitions. This is perhaps due to the presence of two possible nuclear spin allowed rotational relaxation channels (e.g. $1_{11}^- \rightarrow 1_{01}^+$ or 0_{00}^+), having associated energy gaps of ≈7-8 cm^{-1}. The vinyl radical population excited to the 1_{11} level can therefore rotationally relax to an essentially continuous droplet state density.[32, 33] In contrast, the *a*-type transitions access levels that can relax only *via* channels having an energy difference of ≈1.5 cm^{-1}, which corresponds to an energy regime associated with a rather sparse droplet state density.[32, 33] The relative intensities within each set of transitions is ≈3:1, consistent with the predicted nuclear spin weights associated with the exchange of all *three* H atoms, as observed in the jet-cooled spectrum of the ν_3 band.[3] The *a*-type lines are split by the *difference* in the v=0 ($\Delta\tau''$) and v=1 ($\Delta\tau'$) tunneling splittings, and the *b*-type lines are split by the *sum* of these tunneling splittings. From this rather simple spectrum, we can therefore extract the magnitude of the tunneling splittings in both v=0 and v=1. In addition, if we neglect centrifugal distortion, the A'-B' constant is obtained from the separation between the two transitions from the 0_{00}^+ level. The constants and tunneling splittings obtained from the ν_3 band are compared to the gas phase values in Table 3. We also note that the application of a 60 kV/cm electric field to the laser interaction region results in two additional weak peaks at 2902.49 and 2902.60 cm^{-1} (see Fig. S1 of the supporting information).[34] Despite the poor signal to noise ratio associated with this

Stark measurement, which is due to the relatively small dipole moment of the vinyl radical (≈0.5 D), the observed splitting and relative intensities support an assignment of these features to the $0_{00}^{+} \leftarrow 0_{00}^{+}$ and $0_{00}^{-} \leftarrow 0_{00}^{-}$ transitions that are forbidden at zero-field. With this assignment, the ν_3 band origins and the $B'+C'$ constant are obtained directly (see Table 3).

A set of transitions in the survey scan near 3025 cm^{-1} is assigned to the ν_2 CH_2 antisymmetric stretch band, and these are shown in Fig. 6. The ν_2 transitions are broader than the analogous ν_3 lines by a factor of ≈5, despite the fact that the energy gaps associated with the open rotational relaxation channels are similar for both bands. Nevertheless, the *b*-type lines are again approximately three times as broad as the *a*-type transitions, and this broadening washes out the splitting that corresponds to the *difference* in the v=0 and v=1 tunneling splittings. However, with the $\Delta\tau''$ obtained from the analysis of the ν_3 band, a value for $\Delta\tau'$ (ν_2) (0.30(2) cm^{-1}) is obtained directly from the *a*-type transitions, which are split by the *sum* of $\Delta\tau''$and $\Delta\tau'$ (ν_2). With these tunneling splittings and the value of A'-B' (as determined from the ν_3 band), the *b*-type line positions were calculated. These line positions and the relative intensities (from nuclear spin weights) were then fixed in a fit to determine the approximate *b*-type line widths. The results of this fit are shown in Fig. 6 (red line) and are summarized in Table 4. The overall agreement with the expected spectrum strongly supports our assignment of the transitions observed in this region to the ν_2 CH_2 antisymmetric stretch. Furthermore, the ν_2 band origin is within 2 cm^{-1} of the VCI prediction by Bowman and co-workers.[8] We also note that the VCI computations predict an anharmonic resonance between the ν_2 and $3\nu_6$ states, which may be the origin of the broadening observed here for the ν_2 band. For example, a solvent-mediated vibrational relaxation process involving the lower frequency coupled mode (ν_6=1015 cm^{-1}) could lead to an additional lifetime broadening, beyond what is observed for the ν_3 band.

A third band associated with the lone α-CH stretch (ν_1) is predicted by VCI theory to be centered near 3108 cm^{-1}.[8] Harmonic frequencies at the C_s equilibrium geometry were previously computed at the B3LYP/6-311++g(3df,3pd) level of theory, and these indicate that ν_1 could be approximately ten times weaker than the ν_3 band.[3] Because of

this intensity prediction, we carried out a careful survey scan of the lone α-CH stretch region between 3090-3155 cm^{-1}, which is shown in Fig. 7. A number of features between 3100 and 3110 cm^{-1} can be easily identified as transitions belonging to the $2\nu_{10}+\nu_{12}$ and ν_9 vibrational bands of He-solvated C_2H_4.[31] Within the signal to noise limit of the spectrum, no other features near 3110 cm^{-1} are observed that can be assigned to anything other than C_2H_4. Moreover, there are no transitions in the droplet spectrum that fall within 10 cm^{-1} of the peak observed at 3140 cm^{-1} in solid-Ne, which was assigned to the C_2H_3 ν_1 band. A sharp, isolated transition at 3119.6263(1) is observed, which is only present with the pyrolysis source hot, yet is clearly absent in the spectrum of C_2H_4. The region around this transition is shown in Fig. 8. While all experimental conditions suggest that this sharp feature is due to the vinyl radical, the assignment is somewhat less definitive, as this band apparently contains only *one* *a*-type transition. Assuming this transition is an *a*-type line of ν_1, we expect the tunneling splitting to be unresolved if $|\Delta\tau'(\nu_1) - \Delta\tau''|$ is less than about 0.03 cm^{-1}, given the observed line width. Furthermore, given this difference, two *b*-type transitions split by $\approx 2 \times \Delta\tau''$ are expected approximately 6 cm^{-1} to the blue of the unresolved *a*-type transitions. Analogous to the ν_3 band, two broader transitions are indeed observed in the vicinity expected for the *b*-type lines. Nevertheless, the highest frequency transition can be definitively assigned to an impurity species, as this transition gives a strong depletion signal in mass channel 27 u channel, whereas all other transitions assigned to the vinyl radical do not. On the basis of these mass spectrometry measurements, we assign only the peaks at 3119.626 and 3125.24 cm^{-1} to the vinyl radical. A second *b*-type transition is predicted to be near 3124.42 cm^{-1}, with an intensity near the signal to noise limit in the spectrum. The inset to Fig. 8 shows the expected *a*-type transitions, assuming that $\Delta\tau'(\nu_1)$ is either 0.44 cm^{-1} (red) or 0.31 cm^{-1} (blue). The latter value was computed by Nesbitt and Dong using a 1D vibrationally adiabatic *ab initio* potential energy curve along the tunneling coordinate.[7] These *ab initio* computations indicate a significant *decrease* in tunneling splitting upon ν_1 excitation, whereas the droplet spectra indicate a relatively small change, if any. Unfortunately, we are left to speculate as to the origin of the discrepancy between the computed and measured upper state tunneling splitting for ν_1,

and we therefore assign these transitions to the ν_1 band with some reservation, despite the fact that we have found no clear obvious alternative assignment.

IV. Discussion

The band origins of the He-solvated vinyl radical CH stretch vibrations are in rather good agreement with the VCI predictions of Bowman and co-workers.[8] The ν_3 assignment is indeed the most unambiguous of the three, because of the comparison to the high-resolution jet-cooled spectrum. The ν_1 and ν_2 band assignments, while less definitive, are indeed each consistent with the VCI predictions and rotational structure analysis and should therefore provide a suitable starting point for future high-resolution gas phase measurements of these bands. Indeed, recent measurements of other small hydrocarbon radicals isolated in He droplets indicate that in most cases, the CH stretch band origins are only slightly perturbed, with solvent-induced frequency shifts <1 cm^{-1}.[29, 35-37]

A direct comparison of the gas phase and He droplet environments is possible for the tunneling splittings in both the ground state and the excited state of the CH_2 symmetric stretch (ν_3). For both states, $\Delta\tau$ decreases to ≈80% of its gas phase value upon He solvation. Furthermore, the tunneling splitting of the He-solvated vinyl radical unambiguously *increases* upon CH_2 symmetric stretch excitation, and it does so to an extent that, within the error of our measurement, is equivalent to the change observed in the jet-cooled spectrum. The vibrational excitation dependence of $\Delta\tau$ is consistent with Nesbitt and Dong's 1D vibrationally adiabatic *ab initio* computations of the potential surface along the α-CH rocking coordinate.[7] The effective barrier heights of these adiabatically corrected potential surfaces *decrease* by ≈17, 42 or -80 cm^{-1} upon CH_2 symmetric, CH_2 antisymmetric or α-CH stretch excitation, respectively. These changes lead to predicted differences ($\Delta\tau'$-$\Delta\tau''$) in the excited and ground state tunneling splittings of ≈0.075, 0.16 and -0.23 cm^{-1} for ν_3, ν_2 and ν_1, respectively. The agreement between the *ab initio* and experimental gas phase values for $\Delta\tau'(\nu_3)$-$\Delta\tau''$ is promising and justifies a direct comparison of the He droplet $\Delta\tau'(\nu_{2,1})$-$\Delta\tau''$ values to those predicted

by the *ab initio* computations. Nevertheless, the He droplet (-0.11(3) (ν_2), 0.00(3) (ν_1) cm^{-1}) and computed (0.16 (ν_2), -0.23 (ν_1) cm^{-1}) tunneling splitting differences disagree *qualitatively*. Assuming our assignments are valid and the *ab initio* predictions are accurate, the measured droplet splittings imply a $\Delta\tau_{He}/\Delta\tau_{gas}$ ratio of 0.43(15) and 1.3(1) for the ν_2 and ν_1 modes, respectively, whereas the ratio is $\approx$0.8 for *both* the ground state and ν_3 excited state (v=1). It is perhaps unreasonable to expect the droplet effect to differ so dramatically for the three modes probed here. Rather than a solvent effect, the discrepancy may be due instead to the approximations associated with the 1D *ab initio* approach,[7] in which the adiabatic separation between large- and small-amplitude vibrations is assumed to be valid. As noted above, the VCI computations predict a resonance between ν_2 and $3\nu_6$,[8] which could potentially lead to an excited state tunneling splitting that is not accurately captured by the 1D adiabatic computations. Indeed, there are many notable examples in which strong perturbations lead to tunneling splittings that are uncharacteristic of computed effective barrier heights in the excited vibrational state (see Ref. 38 and references therein). This is usually relevant for vibrational modes that are in resonance with combination modes containing a high degree of excitation along the large-amplitude coordinate.[38] The vinyl $3\nu_6$ mode, to which the ν_2 mode is coupled, consists of the in-plane, asymmetric lone α-CH/CH_2 bending motion, which is indeed largely along the large-amplitude contortional coordinate. Additional insight into the origin of the discrepancies between the experimental and computed ν_2 and ν_1 tunneling splittings will have to await high-resolution spectroscopy of the jet-cooled vinyl radical, which these results will hopefully stimulate.

The observed 20% reduction of the ground state and ν_3 excited state tunneling splittings upon He solvation is quite interesting and is likely due to the combination of two effects. On the one hand, the He can directly modify the potential barrier height along the tunneling coordinate, as the solvation energy should depend somewhat on this coordinate. For example, a CCSD(T)/cc-pVTZ calculation predicts the C_2H_3 permanent electric dipole moment to change from 0.67 D to 0.15 D in going from the C_s equilibrium geometry to the C_{2v} transition state, which would lead to a variation in the

dipole induced polarization of the solvent and an effective *increase* in the barrier height along the α-CH rocking coordinate. Previous computations of $\Delta\tau'/\Delta\tau''$,[7] which employ 1D vibrationally adiabatic *ab initio* potentials ($\Delta E_{eff}''$=1602(20) cm^{-1}), show that, over the 1600±100 cm^{-1} range, this ratio scales approximately linearly with the change in effective barrier height upon vibrational excitation. We use this result to estimate the approximate change in barrier height that would be consistent with the $\Delta\tau_{He}/\Delta\tau_{gas}$ ≈0.8 ratio observed here. The corresponding change is a solvent-induced *increase* in the effective barrier of ≈40 cm^{-1}. This likely represents an upper limit, as there is a second solvent effect that cannot be overlooked, namely the solvent-induced modification of the kinetic energy of the tunneling particles. The fluctuating He density in the vicinity of the tunneling molecule necessarily increases the effective moment of inertia associated with this rocking degree of freedom. We computed a CCSD(T)/aug-cc-pVTZ 1D tunneling potential (ΔE=1757 cm^{-1}) to estimate an upper limit for this effect. This potential has been scaled to give the empirically determined effective barrier height of 1602 cm^{-1}. Here we simply assume a constant effective mass along the tunneling coordinate and employ the method of Lin *et al*. to numerically solve the 1D Schrödinger equation.[39] The tunneling splittings obtained in this way are shown in Fig. 9 for a number of effective masses. We find that an increase in effective mass of ≈5% is sufficient to reduce the tunneling splitting by ≈20%. Clearly, even a small solvent contribution to the effective mass of the tunneling particles can result in a significant deviation from the gas phase tunneling frequency. We are hopeful that these results provide a stimulus for theoretical computations of the large amplitude tunneling dynamics of this prototypical hydrocarbon radical that take into account the He solvent effect on both the potential and kinetic energy terms in the Hamiltonian.

V. Summary

The vinyl radical ($H_2C_\beta=C_\alpha H$) has been produced by the pyrolysis of di-vinyl sulfone and trapped in liquid He nanodroplets. At 0.4 K, the entire population of nuclear

spin isomers is cooled to either the 0_{00}^{+} (ortho) or 0_{00}^{-} (para) roconvibrational level. Survey scans in the fundamental CH stretch region reveal three bands that are assigned to the symmetric CH_2 (ν_3), antisymmetric CH_2 (ν_2) and lone α-CH (ν_1) stretch bands. The assignments are based on comparisons to the jet-cooled vinyl radical spectrum of the ν_3 mode,[3] VCI computations of Bowman and co-workers,[8] and the observed rotational fine structure for each band. The vinyl radical CH stretch band origins in He droplets differ from the VCI computations by ≈1, 2 and 10 cm^{-1} for the ν_3, ν_2 and ν_1 modes, respectively.

Each band consists of *a*-type and *b*-type transitions from the 0_{00} level, and each of these is split by either the *difference in* or *sum of* the v=0 and v=1 tunneling splittings. From the separation between and splitting within these *a*- and *b*-type components, we obtain an A'-B' constant and the tunneling splittings in both v=0 and v=1 for each observed band. Comparing the He droplet spectra to previous high-resolution spectroscopy of the ν_3 band,[3] we find that the A'-B' rotational constant for this mode is reduced to 89% of its gas phase value, and the tunneling splittings (ground and ν_3 excited states) are both reduced by ≈20%. In addition, the relative intensities of the ν_3 transitions seem to indicate 4:4 spin statistics for ortho and para nuclear spin isomers, suggesting a facile interchange mechanism for all *three* H atoms within the ≈1200 K pyrolysis source, prior to the pick-up and cooling of the hot vinyl radical by the He droplet. The tentative upper state tunneling splittings extracted from the ν_1 and ν_2 bands are qualitatively inconsistent with those predicted using 1D vibrationally adiabatic potentials along the tunneling coordinate.[7] We currently do not have a clear understanding of this apparent discrepancy, the resolution of which will require high-resolution jet-cooled spectra of these higher frequency bands.

The ≈20% reduction in the ground and ν_3 excited state tunneling splittings is most likely due to two contributing effects from the He solvent. The He droplet can in principle modify both the tunneling barrier and the effective reduced mass for motion along this coordinate. We have estimated that either an ≈40 cm^{-1} increase in the effective barrier height or an ≈5% increase in the effective mass of the tunneling particles (both as upper limits) is sufficient to account for the observed ≈20% tunneling

splitting reduction. Future theoretical work will be required to assess the extent to which each of these effects contribute to the overall modification of the vinyl radical tunneling dynamics upon solvation in liquid He.

Acknowledgements

This work was supported by the Office of Energy Research, Office of Basic Energy Sciences, Chemical Sciences, Geosciences and Biosciences Division of the US Department of Energy (DOE) under Contract No. DE-FG02-12ER16298. We acknowledge partial support from the donors of the American Chemical Society Petroleum Research Fund (50223-DNI6).

References

1. H. Kanamori, Y. Endo and E. Hirota, J. Chem. Phys. **92**, 197-205 (1990).
2. K. Tanaka, M. Toshimitsu, K. Harada and T. Tanaka, J. Chem. Phys. **120**, 3604-3618 (2004).
3. F. Dong, M. Roberts and D. J. Nesbitt, J. Chem. Phys. **128**, 044305 (2008).
4. K. Tanaka, M. Hayashi, M. Ohtsuki, K. Harada and T. Tanaka, J. Chem. Phys. **131**, 111101 (2009).
5. M. Hayashi, K. Harada, R. Lavrich, T. Tanaka and K. Tanaka, J. Chem. Phys. **133**, 154303 (2010).
6. G. V. Mil'nikov, T. Ishida and H. Nakamura, J. Phys. Chem. A **110**, 5430-5435 (2006).
7. D. J. Nesbitt and F. Dong, Phys. Chem. Chem. Phys. **10**, 2113-2122 (2008).
8. A. R. Sharma, B. J. Braams, S. Carter, B. C. Shepler and J. M. Bowman, J. Chem. Phys. **130**, 174301 (2009).
9. A. R. Sharma, J. M. Bowman and D. J. Nesbitt, J. Chem. Phys. **136**, 034305 (2012).
10. L. Letendre, D. -K. Liu, C. D. Pibel, J. B. Halpern and H. -L. Dai, J. Chem. Phys. **112**, 9209-9212 (2000).

11. A. Carvalho, G. Hancock and M. Saunders, Phys. Chem. Chem. Phys. **8**, 4337-4346 (2006).

12. M. Nikow, M. J. Wilhelm and H. -L. Dai, J. Phys. Chem. A **113**, 8857-8870 (2009).

13. R. A. Shepherd, T. J. Doyle and W. R. M. Graham, J. Chem. Phys. **89**, 2738-2742 (1988).

14. Y. -J. Wu, M. -Y. Lin, B. -M. Cheng, H. -F. Chen and Y. -P. Lee, J. Chem. Phys. **128**, 204509 (2008).

15. M. E. Jacox and W. E. Thompson, J. Chem. Phys. **134**, 064321 (2011).

16. M. Hartmann, R. E. Miller, J. P. Toennies and A. Vilesov, Phys. Rev. Lett. **75**, 1566-1569 (1995).

17. K. Nauta and R. E. Miller, J. Chem. Phys. **113**, 10158-10168 (2000).

18. D. Skvortsov, R. Sliter, M. Y. Choi and A. F. Vilesov, J. Chem. Phys. **128**, 094308 (2008).

19. M. Ordlieb, Ö. Birer, M. Letzner, G. W. Schwaab and M. Havenith, J. Phys. Chem. A **111**, 12192-12199 (2007).

20. R. Lehnig, N. V. Blinov and W. Jäger, J. Chem. Phys. **127**, 241101 (2007).

21. P. L. Raston, C. J. Knapp and W. Jäger, Phys. Chem. Chem. Phys. **13**, 18789-18798 (2011).

22. A. Sarsa, Z. Bačić, J. W. Moskowitz and K. E. Schmidt, Phys. Rev. Lett. **88**, 123401 (2002).

23. H. Jiang, A. Sarsa, G. Murdachaew, K. Szalewicz and Z. Bačić, J. Chem. Phys. **123**, 224313 (2005).

24. A. Viel, K. B. Whaley and R. J. Wheatley, J. Chem. Phys. **127**, 194303 (2007).

25. J. P. Toennies and A. F. Vilesov, Angew. Chem.-Int. Edit. **43**, 2622-2648 (2004).

26. M. Y. Choi, G. E. Douberly, T. M. Falconer, W. K. Lewis, C. M. Lindsay, J. M. Merritt, P. L. Stiles and R. E. Miller, Int. Rev. Phys. Chem. **25**, 15-75 (2006).

27. F. Stienkemeier and K. K. Lehmann, J. Phys. B **39**, R127-R166 (2006).

28. E. Knuth, B. Schilling and J. P. Toennies, *Proceedings of the 19th International Symposium on Rarefied Gas Dynamics*. (Oxford University Press, London, 1995).

29. J. Küpper, J. M. Merritt and R. E. Miller, J. Chem. Phys. **117**, 647-652 (2002).

30. A. M. Morrison, T. Liang and G. E. Douberly, Rev. Sci. Instrum. **84**, 013102 (2013).

31. C. M. Lindsay and R. E. Miller, J. Chem. Phys. **122**, 104306 (2005).

32. K. K. Lehmann, J. Chem. Phys. **119**, 3336-3342 (2003).

33. K. Hansen, M. D. Johnson and V. V. Kresin, Phys. Rev. B **76**, 235424 (2007).

34. See Supplementary Material Document No._____ for the preliminary Stark spectra of the ν_3 band, Figure S1.

35. A. M. Morrison, J. Agarwal, H. F. Schaefer III and G. E. Douberly, J. Phys. Chem. A **116**, 5299-5304 (2012).

36. A. M. Morrison, P. L. Raston and G. E. Douberly, J. Phys. Chem. A **117**, DOI: 10.1021/jp3310083j (2013).

37. P. L. Raston, J. Agarwal, J. M. Turney, H. F. Schaefer III and G. E. Douberly, *The ethyl radical in superfluid helium nanodroplets: rovibrational spectroscopy and ab initio computations,* J. Chem. Phys., submitted (2013).

38. A. Ainetschian, G. T. Fraser, J. Ortigoso, and B. H. Pate, J. Chem. Phys. **100**, 729 (1994).

39. C. -K. Lin, H. -C. Chang and S. H. Lin, J. Phys. Chem. A **111**, 9347-9354 (2007).

TABLE I. C_2H_3 vibrational frequencies (cm^{-1}) and relative intensities (in parentheses).

	ν_3	ν_2	ν_1
Gas phase FTIR[a]	3103 (0.05)	3164 (1)	3235 (0.64)
Solid Neon[b]	2911.5 (0.87)	2953.6 (1)	3141.0 (0.67)
Jet-cooled[c]	2901.8603	-	-
Helium[d]	2902.0 (1)	3018.2 (0.9)	3117.6 (0.1)
VCI Theory[e]	2900.7	3015.9	3108.4
Harmonic[f]	3069.7 (1)	3174.0 (0.6)	3242.2 (0.09)

[a] Reference 10. Emission from a photolysis side-product prevented an accurate determination of the line positions in this study.[12]

[b] Reference 14.

[c] Reference 3.

[d] Band origins are determined using gas phase rotational constants and helium droplet line positions. These values thus represent lower limits, and the actual helium droplet band origins could be as much as ≈0.5 cm^{-1} higher, on the basis of preliminary Stark spectroscopy measurements of the $0_{00} \leftarrow 0_{00}$ transitions of the ν_3 band.[34] The value for the ν_1 band origin should be considered as tentative (see text).

[e] Full dimensional Vibrational Configuration Interaction theory, Ref. 8.

[f] Vibrational wavenumbers are from RCCSD(T)/aug-cc-pVTZ theory, Ref. 8. Relative intensities are from B3LYP/6-311++g(3df,3pd) theory, Ref. 3.

TABLE II. Transitions observed in the ν_3 band (CH_2 symmetric stretch).[a]

τ'-τ''	$J'_{Ka'Kc'}$-$J''_{Ka''Kc''}$	Gas phase[b]	He droplet	Relative area	Γ
0^+-0^+	1_{01}-0_{00}	2903.8841	2904.020(1)	1	0.053(3)
0^--0^-	1_{01}-0_{00}	2903.9592	2904.111(2)	0.34	0.043(4)
0^+-0^-	1_{11}-0_{00}	2910.2579	2909.71(1)	0.05	0.14(1)
0^--0^+	1_{11}-0_{00}	2911.3275	2910.62(1)	0.17	0.15(1)

[a] Frequencies (cm^{-1}), relative integrated intensities, and line widths (Γ, cm^{-1}) are determined from Lorentzian fits to helium droplet transitions.

[b] Reference 3. Values for *b*-type lines were calculated using constants.

TABLE III. Tunneling splittings and rotational constants (cm^{-1}) obtained from the ν_3 CH_2 symmetric stretch band.

$\Delta\tau$	gas	He[a]	He/gas[a]
v=0	0.5428[b]	0.41(1)	0.76(2)
v=1	0.6144[c]	0.50(1)	0.81(2)
A'-B'	6.8246[c]	6.10(1)	0.89(1)
B'+C'	2.0253[c]	1.53(2)[d]	0.76(2)
ν_0^+	2901.860	2902.49(2)[d]	-
ν_0^-	2901.932	2902.60(2)[d]	-

[a] Uncertainties are propagated from the uncertainties in the fitted line positions.

[b] Reference 2.

[c] Reference 3.

[d] Obtained from preliminary spectrum of the electric field-induced $0_{00}^+ \leftarrow 0_{00}^+$ transition (see Supporting Information FIG. S1).[34]

TABLE IV. Transitions observed in the ν_2 band (CH_2 antisymmetric stretch).[a]

τ'-τ''	$J'_{Ka'Kc'}$-$J''_{Ka''Kc''}$	He droplet	Relative area	Γ
0^+-0^-	1_{01}-0_{00}	3020.24(10)	0.02	0.37(4)
0^--0^+	1_{01}-0_{00}	3020.96(1)	0.08	0.19(2)
0^--0^-	1_{11}-0_{00}	3026.65[b]	0.33	0.61
0^+-0^+	1_{11}-0_{00}	3026.75[b]	1	0.85

[a] Frequencies (cm^{-1}), relative integrated intensities, and line widths (Γ, cm^{-1}) are determined from Lorentzian fits to the *a*-type helium droplet transitions. The value of $\Delta\tau$ in the ν_2 manifold is equal to 0.30(2) cm^{-1}, and it is derived from the separation between the *a*-type transitions. The upper state $\Delta\tau_{He}/\Delta\tau_{gas}$ ratio equals 0.43(15) if we set the gas phase splitting to the value predicted from vibrationally adiabatic coupled-cluster calculations.[7]

[b] Using $\Delta\tau''$, $\Delta\tau'$ (ν_2) and the value of A'-B' (as determined from the ν_3 band), the *b*-type line positions were calculated. These line positions and the relative intensities (from nuclear spin weights) were then fixed in a fit to determine the approximate line widths. The resulting fit is shown as the red line in Figure 3.

TABLE V. Transitions observed in the ν_1 band (lone α-CH stretch).[a]

τ'-τ''	$J'_{Ka'Kc'}$-$J''_{Ka''Kc''}$	He droplet	Relative area	Γ
0^+-0^+	1_{01}-0_{00}	3119.6263(1)	1	0.0368(1)
0^--0^-	1_{01}-0_{00}	[b]	[b]	[b]
0^+-0^-	1_{11}-0_{00}	[b]	[b]	[b]
0^--0^+	1_{11}-0_{00}	3125.24(1)	0.46	0.10(1)

[a] Frequencies (cm^{-1}), relative integrated intensities, and line widths (Γ, cm^{-1}) are determined from Lorentzian fits to the helium droplet transitions. The $\Delta\tau_{He}/\Delta\tau_{gas}$ ratio $\approx$1.3(1) if we assume no change in tunneling splitting upon vibrational excitation of ν_1, as indicated by the single unresolved *a*-type transition. Here the gas phase splitting corresponds to the value predicted from vibrationally adiabatic coupled-cluster calculations.[7]

[b] Not observed. Here we are assuming the 3119.6263(1) and 3125.24(1) lines are assigned to the $1_{01}^+ \leftarrow 0_{00}^+$ and $1_{11}^+ \leftarrow 0_{00}^+$ transitions, respectively.

Figure Captions:

FIG. 1. Evolution of the helium droplet beam mass spectrum as the pyrolysis source is heated to decompose the di-vinyl sulfone (DVS) precursor. Pyrolytic decomposition of DVS results in a significant increase in ion signal for mass channel m/z=26 u $(C_2H_2)^+$.

FIG. 2. Schematic energy level diagram and allowed transitions for the vinyl radical. Symmetry labeling is based on the C_{2v}(M) molecular symmetry group and assumes a feasible interchange of the two H atom nuclei in the CH_2 group, which proceeds via the tunneling of the lone α-CH bond from one C_s equilibrium geometry to the other through a C_{2v} transition state. At 0.4 K, the two nuclear spin isomer populations are cooled completely to either the 0_{00}^+ level [ortho ($\Gamma_{ns}=A_1$)] or the 0_{00}^- level [para ($\Gamma_{ns}=B_2$)]. The splitting between the lower (+) and upper (-) tunneling levels is exaggerated. The spin weight ratios will be 4:4 if there is a mechanism for the feasible exchange of all three H atoms (see text).

FIG. 3. Survey scan in the CH stretch region. Ion signal depletion is measured in mass channel m/z=26 u. Arrows indicate peaks assigned to the vinyl radical. Almost all of the remaining intensity is attributed to helium solvated ethylene.[31] An intense precursor (DVS) peak at 3033.62 cm^{-1} is completely absent in this spectrum, indicating both the extent of DVS decomposition and the selectivity associated with the m/z=26 u mass channel.

FIG. 4. Difference mass spectrum (Laser OFF-ON) obtained with the laser frequency fixed to the peak of the ν_3 $1_{01}^+ \leftarrow 0_{00}^+$ transition at 2904.02 cm^{-1}. A single mass channel (m/z=26 u) carries almost all of the signal associated with the laser-induced depletion of droplets containing single vinyl radicals.

FIG. 5. Spectrum of the ν_3 CH_2 symmetric stretching band, showing both *a*-type and *b*-type components. The four observed transitions are assigned to those shown schematically on the left-hand side of Fig. 2. The *a*-type transitions are shown as the inset. The red curve is a simulation based on the constants reported in Table II.

FIG. 6. Spectrum of the ν_2 CH_2 antisymmetric stretching band, showing both *a*-type and *b*-type components. The observed transitions are assigned to those shown schematically on the right-hand side of Fig. 2. The red curve is a simulation based on the best fit parameters reported in Table IV (see Table IV caption for details).

FIG. 7. Survey scan in the lone α-CH stretching region (mass channel 26 u). Vertical arrows indicate peaks assigned to the vinyl radical. The peak marked by an asterisk is due to an unidentified impurity. The remaining depletion signal is attributed to helium solvated ethylene.[31]

FIG. 8. Spectrum assigned to the ν_1 lone α-CH stretch band, showing the *a*-type and *b*-type lines. The bottom red simulation assumes no change in tunneling splitting upon vibrational excitation and an $A'+B'$ constant of 5.61 cm^{-1}. The single *a*-type transition is shown as the inset, along with simulations of the predicted spectrum assuming either a v=1 tunneling splitting of 0.44 cm^{-1} (red) or the value predicted by Nesbitt *et al*. (blue, 0.31 cm^{-1}).[7] The peak marked by an asterisk is due to an unidentified impurity.

FIG. 9. Tunneling splitting versus effective reduced mass, assuming a 1D potential along the in-plane α-CH rock coordinate. The CCSD(T)/aug-cc-pVTZ potential is scaled to reproduce the empirically determined 1602 cm^{-1} barrier height. An ≈5% increase in effective reduced mass reproduces the observed ≈20% decrease in tunneling splitting.

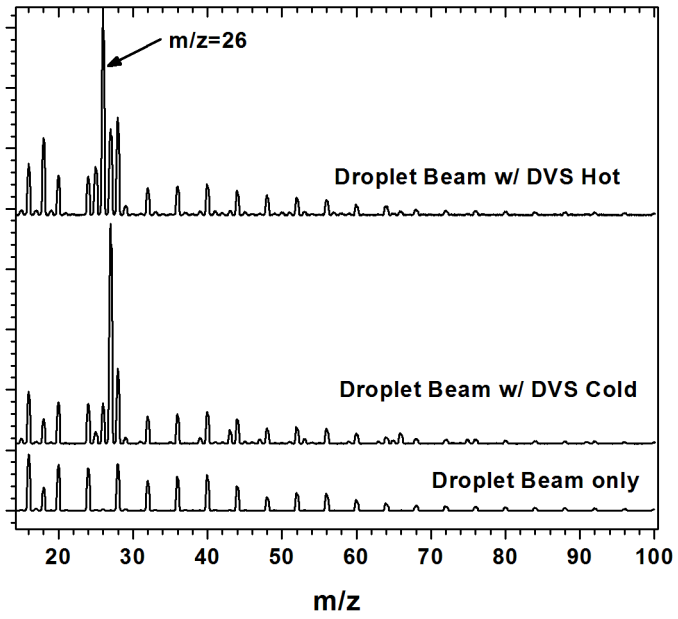

Figure 1

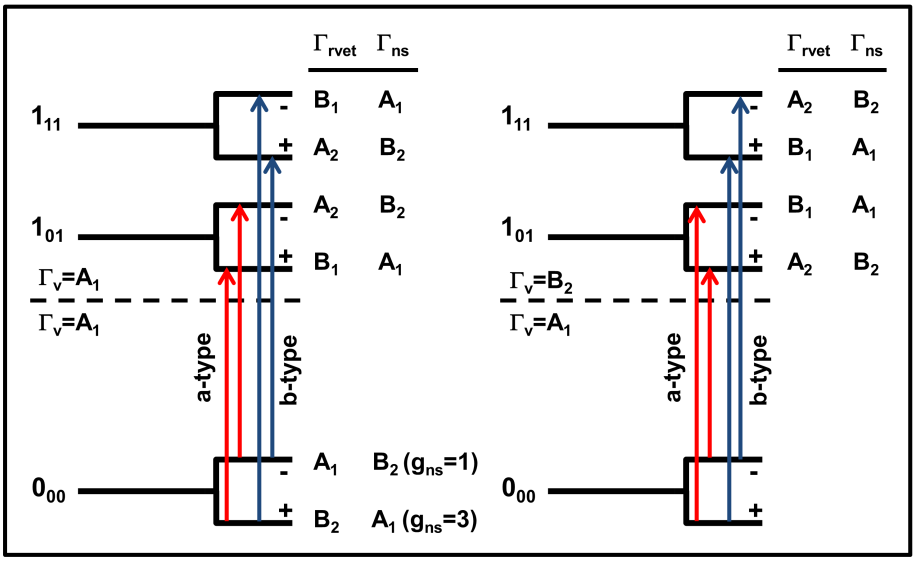

Figure 2

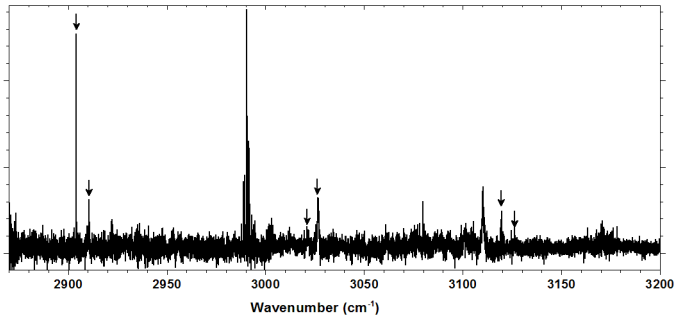

Figure 3

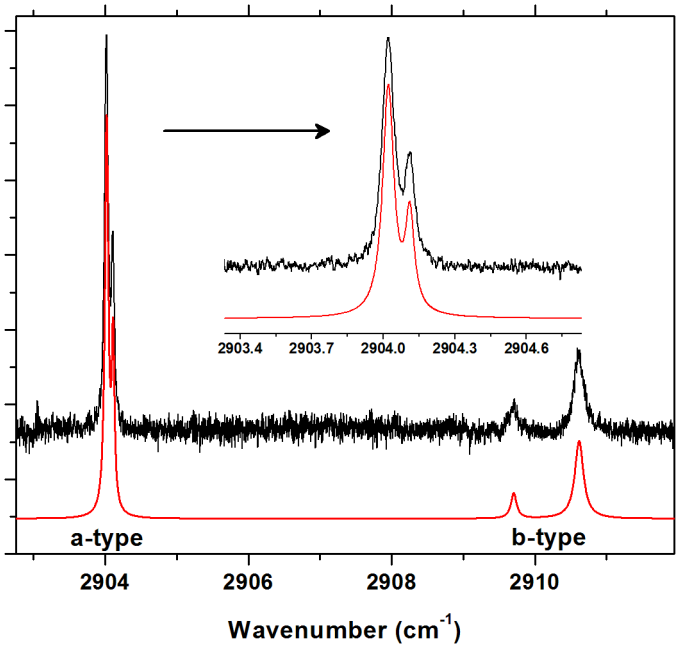

Figure 4

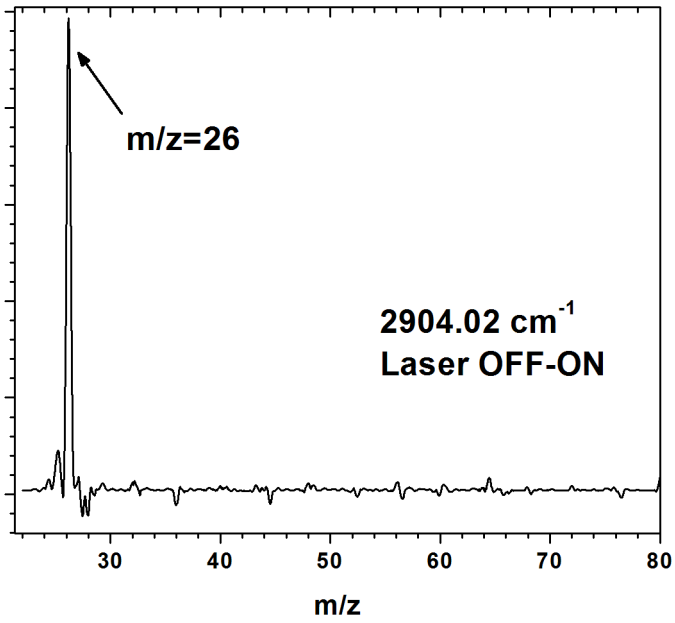

Figure 5

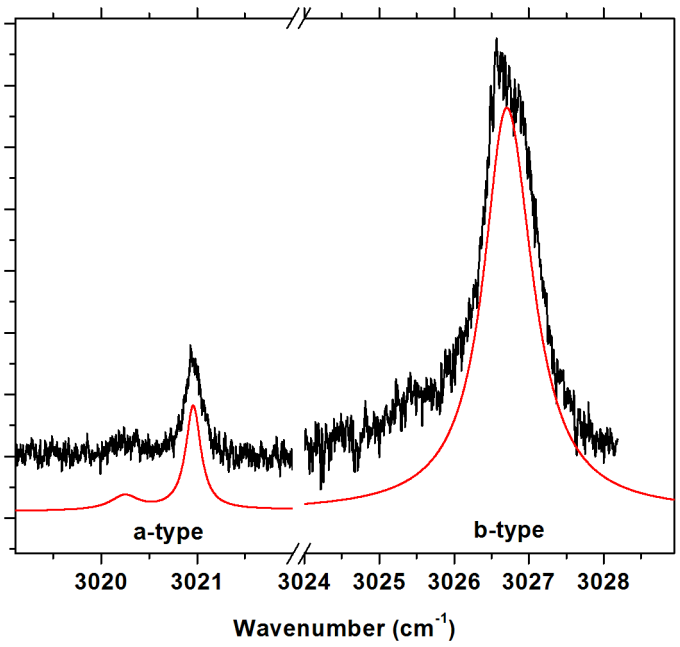

Figure 7

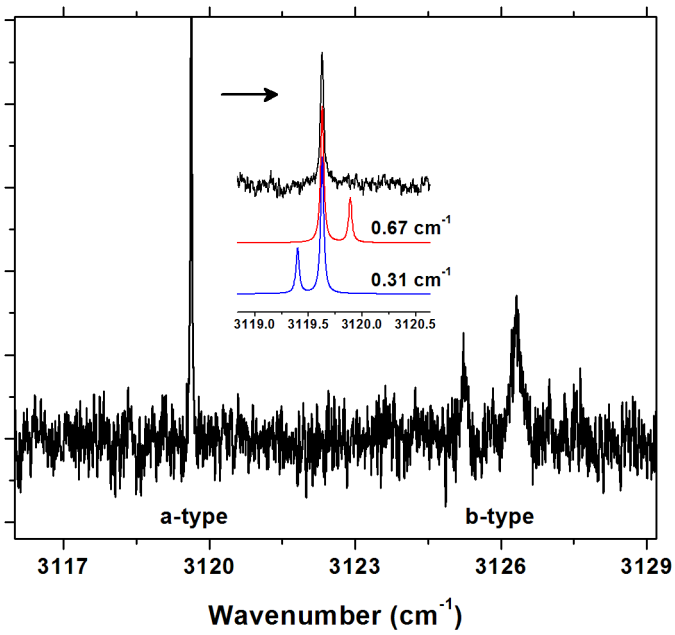

Figure 8

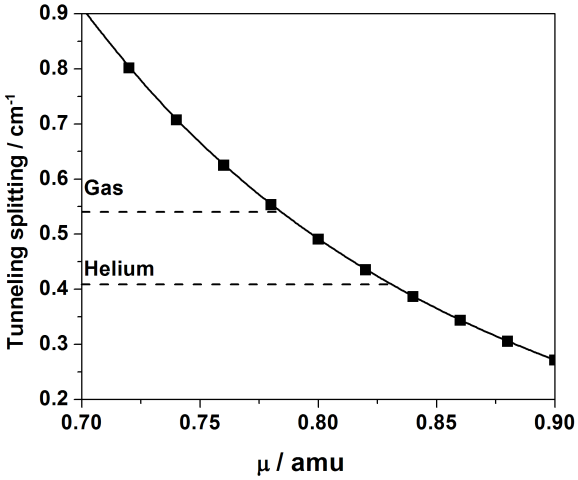
Tunneling splitting / cm-1
0.9
0.8
0.7
0.6
0.5
0.4
0.3
0.2
Gas
Helium
0.70
0.75
0.80
0.85
0.90
μ / amu

Figure 9